In situ molecular NMR picture of bioavailable calcium stabilized as amorphous $CaCO_3$ biomineral in crayfish gastroliths

Anat Akiva-Tal[a], Shifi Kababya[a], Yael S. Balazs[a], Lilah Glazer[b,c], Amir Berman[c,d], Amir Sagi[b,c], and Asher Schmidt[a,1]

[a]Schulich Faculty of Chemistry and Russell Berrie Nanotechnology Institute, Technion—Israel Institute of Technology, Haifa 32000 Israel; [b]Department of Life Sciences, Ben-Gurion University of the Negev, Beer Sheva 84105, Israel; [c]The National Institute for Biotechnology in the Negev, Beer Sheva 84105, Israel; and [d]Department of Biotechnology Engineering and Ilse Katz Institute for NanoScience and Nanotechnology, Ben-Gurion University of the Negev, Beer Sheva 84105, Israel

Edited by Harry B. Gray, California Institute of Technology, Pasadena, CA, and approved July 12, 2011 (received for review February 16, 2011)

Bioavailable calcium is maintained by some crustaceans, in particular freshwater crayfish, by stabilizing amorphous calcium carbonate (ACC) within reservoir organs—gastroliths, readily providing the Ca^{2+} needed to build a new exoskeleton. Despite the key scientific and biomedical importance of the in situ molecular-level picture of biogenic ACC and its stabilization in a bioavailable form, its description has eluded efforts to date. Herein, using multinuclear NMR, we accomplish in situ molecular-level characterization of ACC within *intact* gastroliths of the crayfish *Cherax quadricarinatus*. In addition to the known $CaCO_3$, chitin scaffold and inorganic phosphate (Pi), we identify within the gastrolith two primary metabolites, citrate and phosphoenolpyruvate (PEP) and quantify their abundance by applying solution NMR techniques to the gastrolith "soluble matrix." The long-standing question on the physico-chemical state of ACC stabilizing, P-bearing moieties within the gastrolith is answered directly by the application of solid state rotational-echo double-resonance (REDOR) and transferred-echo double-resonance (TEDOR) NMR to the intact gastroliths: Pi and PEP are found molecularly dispersed throughout the ACC as a solid solution. Citrate carboxylates are found <5 Å from a phosphate (intermolecular C···P distance), an interaction that must be mediated by Ca^{2+}. The high abundance and extensive interactions of these molecules with the ACC matrix identify them as the central constituents stabilizing the bioavailable form of calcium. This study further emphasizes that it is imperative to characterize the intact biogenic $CaCO_3$. Solid state NMR spectroscopy is shown to be a robust and accessible means of determining composition, internal structure, and molecular functionality in situ.

biomineralization | stabilized amorphous calcium carbonate

Calcium carbonates have enormous importance within the field of biomineralization. Within numerous organisms the ability to tailor the biomineralization of calcium carbonate to achieve a variety of functionalities, e.g., structural-mechanical, optical, storage has evolved (1, 2). These organisms exert exquisite control over the mineral production process, from the initial steps of clustering and/or prenucleation—through bulk formation with the desired composition, polymorph, and morphology—to the higher hierarchical arrangement of the final biomineralized material (3, 4). In this process inorganic and bioorganic agents are involved, including biomacromolecules (e.g., proteins and polysaccharides) (5–7), serving diverse roles of regulation and control. En route to the formation of the final biomineral, an evolutionarily favored set of these agents—inorganic ions, bioorganic molecules, and proteins—are entrapped at specific levels and become an integral part of the resulting biomineral, in effect tuning the final (targeted) properties that enable functionality (8). Organisms accomplish this high-level synthesis, intra- or extracellularly, at ambient conditions and, by far, exceed all current state-of-the-art synthetic capabilities.

There are five crystalline polymorphs of $CaCO_3$, yet the amorphous form, amorphous calcium carbonate (ACC)—thermodynamically the most unstable and most soluble form with wide structural variability, was shown to play the most critical and diverse roles in the mode of action of biomineralization. For instance, ACC has been shown to serve as a transient form designed to spontaneously evolve into a preset specific crystalline form with sculptured morphology (9–11). It has also been shown that ACC can be stabilized to remain in a highly soluble amorphous state, in which case the calcium can be readily retrieved, thus establishing its bioavailability (12, 13). These properties of ACC attract extensive scientific, technological, and biomedical interest. However, the detailed molecular modes of interaction of various additives that are implicated in ACC stabilization, such as phosphate, magnesium (14) and phosphorylated proteins, are as yet unidentified. One inherent difficulty is that the lack of long-range order in amorphous systems impedes structural data obtained through diffraction. Thus, in vitro (15–17) experiments or alterations of the biogenic structures (18) have been turned to in order to gain knowledge of the "individual" roles of such agents (alone and together). Although the importance of such approaches for materials science cannot be overestimated, they cannot directly address the characterization of the intact biogenic matter. Because of this difficulty, identifying the central chemical agents involved in stabilization of ACC in situ, e.g., organic vs. inorganic phosphates, and whether present as separated phases or in a form of solid solutions, has remained a long-standing open question (9). In order to gain insight into the interactions of these agents with the $CaCO_3$ host, and to establish the mechanisms of stabilization, it is imperative to study these biogenic systems as they are, intact and unperturbed, in situ.

Solid state NMR, being a highly local probe of molecular environment, not hindered by lack of long-range order, *and* nonperturbing to the chemical state of the system, stands as one of the most powerful techniques for studying the internal, fine structure of biogenic materials in situ. Recently, employing solid state NMR techniques, we have shown (19) that coccolithophores (*Emiliania huxleyi*, *Pleurochrysis carterae*, and *Gephyrocapsa oceanica*) actively direct the incorporation of minute quantities ($\lesssim$0.1 mol %) of inorganic phosphate (Pi) and nitrate into their sculpted calcitic coccoliths (20). The inorganic anions were shown to be incorporated as intracrystalline structural defects that do

Author contributions: A. Schmidt designed research; A.A.-T., S.K., and Y.S.B. performed research; L.G., A.B., and A. Sagi handled crayfish growth and gastroliths extraction; A.A.-T., S.K., Y.S.B., and A. Schmidt analyzed data; and A. Schmidt wrote the paper with input from all authors.

The authors declare no conflict of interest.

This article is a PNAS Direct Submission.

[1]To whom correspondence should be addressed. E-mail: chrschm@tx.technion.ac.il.

This article contains supporting information online at www.pnas.org/lookup/suppl/doi:10.1073/pnas.1102608108/-/DCSupplemental.

not disrupt the "perfect" calcite structure, yet induce reduced lattice rigidity across about a fifth of the entire bulk crystalline material. These fine in situ solid state NMR observations selectively detect intermolecular interfaces within the biomineral bulk. Inspired by this characterization, we have exploited and tailored these insightful, yet robust, NMR techniques to elucidate the molecular details of how the fresh water crayfish *Cherax quadricarinatus* stabilizes bioavailable calcium. Both the amorphous form (compared to crystalline) and the inability to enrich the gastroliths with stable isotopes (as employed to enhance sensitivity of the coccoliths) make this study far more demanding.

Biomineralization in crustaceans is a subject of intensive study (21) due to the key role of calcium metabolism in the periodic shedding of the exoskeleton and its subsequent replacement. Several crustacean species form temporary extracellular calcium carbonate storage deposits during the premolt stage (22). In freshwater crayfish, including our subject organism—*C. quadricarinatus*, these deposits include a pair of disc-like structures known as gastroliths that are located on each side of the stomach wall (23). In these calcium reservoirs $CaCO_3$ is deposited on a chitin scaffold and is stabilized as ACC (24). Crustaceans in general take advantage of the higher solubility of the ACC (25) with the calcium readily bioavailable for deposition onto a newly formed exoskeleton. These gastroliths contain high phosphorous levels (up to 18 mol % P/Ca) (9, 26, 27) and a number of proteins (approximately 1 wt %), with only a few highly phosphorylated (17, 28–32). All constituents may be implicated in the ACC stabilization. In particular, the highly phosphorylated gastrolith proteins, as well as phosphoserine and phosphothreonine, were shown to induce the formation of stable ACC in vitro (17). Parallel to the current report, the presence of small molecular weight metabolites [phosphoenolpyruvate (PEP), 3-phosphoglycerate (3PG), and citrate] were identified in the exoskeleton and gastroliths of the crayfish *Procambarus clarkii*, (33) and using in vitro experiments their relative potency to induce stabilized ACC formation were shown. In our work, applying solution NMR to the soluble fraction of the gastrolith, we identify the major small molecular weight components that are integrated within the gastrolith—Pi, PEP, and citrate—and quantify their levels. Applying solid state NMR to the intact gastrolith we identify their molecular interactions with the ACC matrix in situ and determine their individual roles in stabilizing bioavailable calcium. These direct observations further emphasize the critical importance of in situ characterization (compared to in vitro) when studying complex biogenic materials.

Results and Discussion

Gastrolith Composition. The composition and structural characteristics of the intact gastrolith are first addressed by solid state ^{13}C NMR (Figs. 1 *A*–*C*). The major component, ACC, is clearly identified by its carbonate peak seen in the ^{13}C direct excitation (DE) magic angle spinning (MAS) spectrum (Fig. 1*A*) of the *intact* gastrolith (Fig. 1*D*). This fully relaxed spectrum (Fig. 1*A*) reports quantitatively all carbon species present in the unperturbed solid. The absence of any other peaks of coexisting bioorganic content from the spectrum implies they are below the spectral noise level (approximately 5%) and clearly indicates that the carbonate carbons (of $CaCO_3$) are the most abundant carbon constituent in the gastrolith. The carbonate peak is centered at 168.6 ppm, calcite chemical shift, and its width is 3.5 ppm (FWHM). The large peak width reflects the extent of the distribution of chemical environments and local order around that of calcite, typical of disordered systems including synthetic ACC. The chemical shift and the very broad linewidth therefore identify the $CaCO_3$ as ACC, with an average short-range order similar to that of calcite. Such a direct interpretation is well established and within the spectral resolution of ^{13}C solid state NMR (34–37) and has been well correlated with X-ray absorption spectroscopy

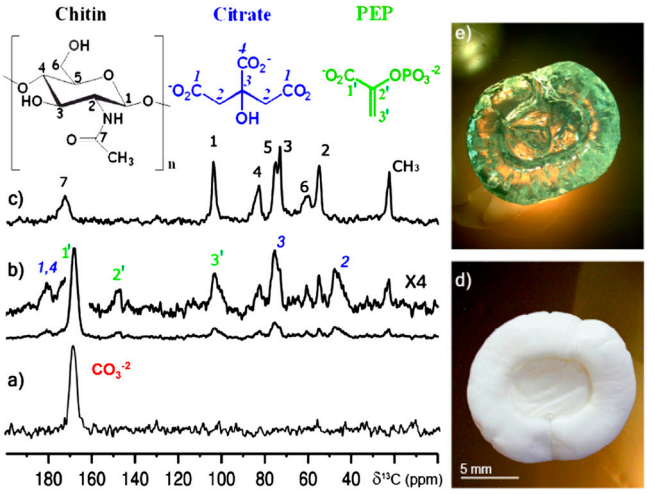

Fig. 1. ^{13}C MAS NMR spectra of intact gastrolith of the crayfish *C. quadricarinatus* (*A* and *B*) and of the decalcified gastrolith (*C*). (*A*) DE MAS, fully relaxed spectrum (40-min repetition delay); (*B*) CP MAS spectrum and its vertical expansion (×4) with peak assignment of the bioorganic content. (*C*) CP MAS spectrum of the decalcified gastrolith showing the insoluble matrix. (*Top*) Molecular structures of the chitin repeat unit and of PEP and citrate. (*D* and *E*) Photos of the intact and of the decalcified gastrolith.

(11, 38, 39). In order to enhance carbon peaks arising from the bioorganic (hydrogen-rich) content of the gastrolith, ^{13}C CP (cross-polarization) MAS NMR spectroscopy was employed. This gives rise to a spectrum (Fig. 1*B*) in which an intense ACC carbonate peak and a collection of bioorganic carbon peaks appear. The similarity of the carbonate peak between the CP and the DE ^{13}C MAS experiments indicates that all carbonate environments are uniformly represented by CP and that they all reside in hydrogen-rich environments. This observation is consistent with the fact that stabilized biogenic ACC is highly hydrated ($CaCO_3$:H_2O = 1:1) (35, 40).

In addition to this most pronounced carbonate peak, the ^{13}C CP MAS spectrum (Fig. 1*B*, vertical expansion) of the intact gastrolith reveals a large set of peaks that arise from its bioorganic content. The identification of the molecules that give rise to these peaks and their complete assignment was done by combining solid state and solution NMR techniques. Decalcification of the intact gastrolith by its immersion in an EGTA solution dissolves the $CaCO_3$ and some of the matter contained within it, creating a solution denoted "soluble matrix" (*SI Text*). The chitin scaffold and nonsoluble matter left behind as a solid is denoted the "insoluble matrix" (Fig. 1*E*). The ^{13}C CP MAS spectrum of the rinsed and dried insoluble matrix (Fig. 1*C*) is that of α-chitin, known to constitute the gastrolith polysaccharides scaffold (25, 41). All chitin peaks are also seen in the spectrum of the intact gastrolith (Fig. 1*B*). The soluble matrix was then characterized by 1D and 2D multinuclear (^1H, ^{13}C, and ^{31}P) solution NMR spectroscopy as described in detail in *SI Text*. This characterization resulted in the identification of the primary metabolites PEP and citrate, in addition to Pi. Their identification was confirmed by spiking experiments with PEP, citrate, and Pi (*SI Text*). Peaks that arise from PEP and citrate are clearly seen for the intact gastrolith (Fig. 1*B*); however, they are absent from the spectrum of the insoluble matrix (Fig. 1*C*). These observations therefore locate PEP and citrate primarily in the soluble matrix. If they also occur within the insoluble matrix, their residual levels are below the experimental sensitivity. PEP and citrate are primary metabolites, of which only citrate is well known in connection with biomineralization activity for its ability to chelate calcium ions (12, 42).

The phosphorous content of the intact gastrolith, apparent in the ^{31}P CP MAS spectrum (Fig. 2*A*, *Bottom*), is expressed

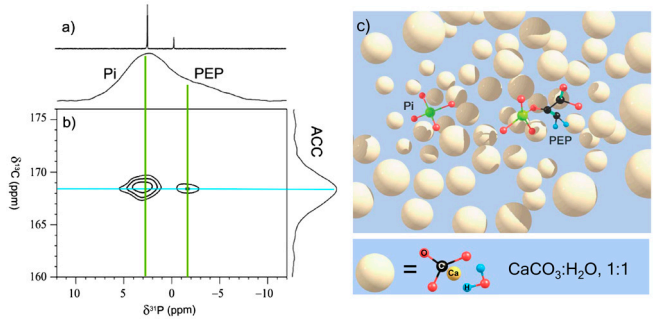

Fig. 2. (*A*) ^{31}P NMR spectra. (*Bottom*) 121.5-MHz CP MAS spectrum of intact gastrolith of *C. quadricarinatus* showing two partially resolved peaks assigned to Pi and PEP. (*Top*) 161.3-MHz solution NMR of the soluble matrix. Solution chemical shift values of phosphates are pH dependent and are different from the in situ values (*SI Text*). (*B*) ^{31}P → ^{13}C 2D-HETCOR MAS NMR spectrum of intact gastrolith of the crayfish *C. quadricarinatus* showing connectivity between Pi to ACC carbonate and between PEP phosphate to ACC carbonate. ^{1}H to ^{31}P contact time of 2 ms and $24 \times 24T_R$ TEDOR mixing were employed. (*C*) A schematic drawing of ACC with Pi and PEP molecularly dispersed.

as two main, partially resolved peaks. The increased resolution of the ^{31}P solution NMR spectrum of the soluble matrix (Fig. 2*A*, *Top*) clearly shows both peaks, identified as Pi and PEP (*SI Text*). Our characterization of different gastroliths showed that the total P content in the "soluble" fraction was found to vary between 6 and 18 P/Ca mol %, a range similar to an earlier inductively coupled plasma atomic emission spectroscopy (ICP-AES) report (17). The Pi level within the soluble fraction was 4–16 mol % (Pi/Ca), whereas the PEP level was 0–4 mol %. Relative PEP/Pi ratios varied in the range of 0–70% (*SI Text*, p. 5).

The fact that also in the absence of PEP the characteristics of the ACC were alike in all gastroliths indicates that Pi is the critical constituent employed by the organism for ACC stabilization. PEP may therefore play additional roles and the dependence of its abundance within the gastrolith on other factors is the subject of a separate study. Variability of citrate levels in all gastroliths analyzed was 2–4 citrate/Ca mol % (*SI Text*, p. 5). It is noted that the low level of additional known proteinaceous content of the gastrolith (28, 29) is below our current experimental sensitivity. Independent of the current work, the presence of PEP, 3PG, citrate, and phosphate in the exoskeleton and the gastroliths of *P. clarkii* was reported (33). Following this report, further examination of our solution NMR spectra showed detectable peaks consistent with 3PG for only a small number of the gastroliths, albeit their very low intensities indicate a much lower concentration than Pi or PEP. Interestingly, the total P/Ca mol ratio for *P. clarkii* reaches only 4%, a value that is much lower than found in *C. quadricarinatus* (18%). Future study will aim at in-depth characterization of this wide variability across organisms.

Internal Structure of the Gastrolith ACC. Having the molecular agents within the gastrolith identified, the next step is to gain insight into how they are chemically and physically organized to stabilize the bioavailable calcium. To probe for spatial proximity (<6 Å) between the ACC carbonates and either Pi or PEP, we used a 2D NMR experiment, ^{31}P → ^{13}C 2D-HETCOR (heteronuclear correlation) ($24 \times 24T_R$ TEDOR (transferred-echo double-resonance) mixing, *SI Text*) (43–45). The 2D-HETCOR NMR spectrum (Fig. 2*B*) clearly shows a cross-peak between both Pi and PEP to the carbonate of ACC. This suggests that both species are molecularly dispersed within the ACC, as is illustrated schematically in Fig. 2*C*.

For a more comprehensive and quantitative evaluation, we turn to rotational-echo double-resonance (REDOR) NMR spectroscopy (19, 46), a solid state NMR technique that enables identification of all carbon species—carbonates and bioorganics—that interact with P atoms of P-bearing molecules. Moreover, interatomic distance constraints of the occurring intermolecular geometry can be determined. The $64T_R$ ^{13}C{^{31}P} CP-REDOR reference spectrum (Fig. 3*A*; S_0) of the intact gastrolith shows all ^{13}C carbons, as seen previously in the ^{13}C CP MAS spectrum (Fig. 1*B*, vertical expansion). Its REDOR difference spectrum (Fig. 3*B*; ΔS) reveals only those carbons (of all molecular components) that lie within *ca.* 9 Å of a phosphorous atom of Pi or PEP; 9 Å is the maximal detectable distance (*SI Text*, p. 1). Most pronounced in this REDOR difference spectrum is the carbonate peak (Fig. 3*C*) whose relative intensity, $\Delta S/S_0$, is about 50%. This observation indicates that over half of the carbonate carbons of ACC report such proximity. Conducting the REDOR experiment as a function of REDOR dipolar evolution time shows a monotonic increase (Fig. 3*D*) of the carbonate difference peak ($\Delta S/S_0$). These observations can be interpreted only in terms of a phosphorous—the minor component of the gastrolith—being molecularly dispersed within the major component—ACC. The envisioned situation of a phosphorous (Pi, PEP) surrounded by a "sea" of carbonates indicates a distribution of ^{31}P···^{13}C distances. Calculated REDOR evolution curves (*SI Text*, p. 2) for model spheres of $CaCO_3:H_2O$ (1:1) where a ^{31}P is placed at their center show that spheres of 8–9 Å radii agree well with the experimental data (Fig. 3*D*). The unequivocal conclusion then is that phosphorous-bearing molecules are dispersed *within* the entire *ACC*, with most carbonates within 8–9 Å from a phosphorous atom.

This evidence distinctly describes a solid solution of P within ACC, as opposed to separate phases, thus cleanly resolving a long-standing question (9). We emphasize that the resulting structural description of the ACC is a comprehensive one. The presence of a single P moiety within the ACC sphere of 8–9 Å radius is straightforwardly translated into a capacity of P/Ca~ 3–4 mol %. Because the average P concentration in the gastroliths of *C. quadricarinatus* is significantly higher (up to 18 mol %) and nonuniform (2–25 mol % from energy dispersive spectro-

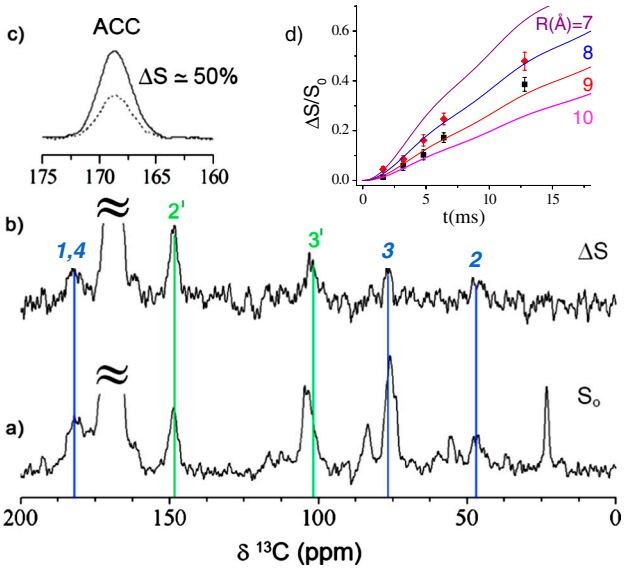

Fig. 3. ^{13}C{^{31}P} CP-REDOR MAS NMR spectra ($64T_R$; 12.8 ms) of intact gastrolith of the crayfish *C. quadricarinatus*. (*A*) S_0 reference spectrum: accounts for all carbon species; (*B*) ΔS difference spectrum: shows peaks only for species that are within 9 Å from a P atom of Pi or PEP. (*C*) Expanded carbonate region: shows a 50 ± 2% REDOR difference peak. (*D*) Experimental (points; two gastroliths) and simulated REDOR $\Delta S/S_0$ evolution curves; simulations are for 1:1 $CaCO_3:H_2O$ spheres ($R = 7$, 8, 9, 10 Å) with a central P atom, accounting for ^{13}C···^{31}P distance distribution (*SI Text*).

scopy measurements) (17), the emerging conclusion is that *excess* of P-rich phases must be present as well. It has been previously reported that separated phases of amorphous calcium phosphate occur in calcium storage structures of the terrestrial crustacean *Orchestia cavimana* (17, 47).

In order to focus on the bioorganic content and identify its interactions with phosphorous-bearing moieties, we examine the remaining ^{13}C NMR peaks from the $^{13}C\{^{31}P\}$ CP-REDOR experiment (Fig. 3 *A* and *B*). The three carbons of the abundant phosphorylated metabolite, PEP, bear *intramolecular* proximity to the phosphate. C_2, the closest (approximately 2.7 Å) to the phosphate of PEP, shows the expected 100% REDOR difference peak (148.5 ppm). The C_1 and C_3 resonances of PEP (172 and 103 ppm, respectively) are overlapped by the peaks of carbonate ACC and C_1 of chitin, respectively, and therefore the relative intensity of their REDOR peaks cannot be accurately determined. Next, the citrate carboxylates (C_1 and C_4, centered at 182 ppm) exhibit a REDOR difference peak of $75 \pm 5\%$ (Fig. 3). The other citrate carbons, C_2 and C_3, also show REDOR difference peaks; however, they cannot be quantified due to the limited S/N and the partially overlapping chitin peaks. The geometric implication of the REDOR data for the carboxylate carbons is that either 75% of them are approximately 4.5 Å from ^{31}P species, or all are approximately 5 Å from P species (*SI Text*, p. 2). This tight intermolecular arrangement of the citrate carboxylates with Pi and/or PEP phosphate, both being negatively charged, must be mediated by a cation, a likely candidate being the most abundant Ca^{2+}. Whether also citrate is dispersed within the ACC or present as a separated phase cannot be determined by the current data.

Conclusions

This study unravels the low molecular weight content of intact gastroliths from *C. quadricarinatus* and quantitatively determines the abundance of the different major constituents (Pi, PEP, and citrate). Exposing their molecular interactions with the intact ACC matrix, it also elucidates the role of each species in stabilizing bioavailable calcium as ACC. The methodological approach, applying primarily solid state NMR spectroscopy to the intact biomineral in situ and solution NMR to the soluble fraction, proves to be most informative and widely applicable to biogenic systems.

The emerging structural description of gastrolith ACC is of carbonates whose immediate local environments span high heterogeneity, yet are "colored" by the chemical identity and short-range order similar to that of calcite. These environments are hydrogen-rich, consistent with the high hydration of biogenically stable ACC, within which Pi and PEP are molecularly dispersed in a form of a solid solution. Their widespread occurrence and extent of intermolecular interactions with the ACC is therefore concluded to be the dominant factor in stabilizing the amorphous $CaCO_3$. An earlier study showed that gastrolith phosphoproteins, some of their phosphorylated proteolysis products as well as single phosphor-amino acids, can induce ACC formation and stabilization in vitro, whereas their nonphosphorylated counterparts did not have such effects (17). Demonstrating the importance of phosphate and phosphorylation in vitro led to attribute in situ induction and stabilization of ACC to those phosphoproteins. However, the abundance of the putative phosphorylated residues of gastrolith proteins (proteins make 1 wt % of the gastrolith with only a few showing phosphorylation level up to 12%) is very low compared to that of Pi and PEP. The role of gastrolith proteins may therefore be complementary to ACC stabilization. This conclusion is further supported by the report of Sato et al. identifying the small molecular weight metabolites—PEP, 3PG, and citrate, in addition to Pi, in the exoskeleton and gastroliths of a different freshwater crayfish, *P. clarkii* (33). Conducting in vitro precipitation experiments of calcium carbonate in the presence of soluble gastrolith extracts that are below or above 10 kDa, they have found that stabilized ACC is formed only in the presence of the low molecular weight (MW) content, suggesting that only the low MW constituents, and not the high MW gastrolith proteins, serve for ACC stabilization. Conducting coprecipitation experiments of calcium carbonate with either Pi, or PEP, or 3PG, they showed that both PEP and 3PG are more efficient than Pi in inducing stable ACC precipitation and attributed this observation to its more critical role. However, our in situ measurements that were performed on a large set of gastroliths (*C. quadricarinatus*) clearly showed that the stabilized ACC is formed also in the absence of PEP, therefore identifying the Pi component as playing the most critical role in achieving the functional ACC material. The in vitro coprecipitation experiments of Sato et al. reflect the high mismatch of PEP and 3PG vs. the high solubility of Pi when coprecipitated with calcium carbonate. Their in vitro *potency* to induce ACC does not reflect their in situ importance. Although these metabolites clearly contribute to the resulting stabilization of the bioavailable calcium form, their primary role must be attributed to the activation of the metabolic machinery within a rapidly forming organ [approximately 14 d (48)] as the gastrolith. This comparison further emphasizes that comprehensive understanding of a complex biogenic matter must be obtained via in situ characterization.

Citrate, the second primary metabolite that we identified in significant amounts within the intact *C. quadricarinatus* gastroliths, is found in situ to be in close proximity to P species (PEP and/or Pi), an interaction that must be mediated by a divalent cation, with most abundant Ca^{2+} being the most probable candidate. The primary metabolite citrate may therefore have two functional roles: (*i*) to bind Ca^{2+} and then, thereby, P moieties, and (*ii*) given its high affinity to Ca^{2+}, to facilitate calcium transport between the exoskeleton and the gastrolith. Delineating whether these "complexes" of citrate-Ca^{2+}-P species are dispersed within the ACC, contributing to its stabilization or residing phase separated from the ACC is the aim of our continuing work.

This NMR study of ACC in gastroliths, along with the earlier study of coccoliths calcite, spans two biogenic systems representative of rare extremes: thermodynamically metastable amorphous $CaCO_3$ vs. the most stable crystalline polymorph, and extra- vs. intracellular synthesis. The NMR characterization shows how each organism, by fine-tuning the P-level incorporation directs and stabilizes very different functional structures of calcium carbonate. The in situ application of routine and robust NMR techniques in a straightforward manner to obtain unique, molecular-level insights into the structural organization of inorganic and small bioorganic molecules within the ACC enabling its stabilization should influence further research and applications ranging from rational design of functional materials to methodologies to enhance calcium bioavailability.

Methods

Gastrolith Sample Preparation. ***Animals and molt.*** *C. quadricarinatus* males were grown in artificial ponds at Ben-Gurion University of the Negev under the conditions described in Shechter et al. (25). Intermolt crayfish were held in individual cages and endocrinologically induced to enter premolt through removal of the X organ–sinus gland complex or ecdyson injections (28). The progression of the molt cycle was monitored daily by measuring gastrolith molt mineralization index (MMI), as described by Shechter et al. (48). Gastrolith dissection was performed around day 1 when MMI was 1.4–1.5. For all dissection procedures, crayfish were placed on ice for 5–10 min until they were anesthetized. Gastroliths were rinsed with water and then kept at ambient conditions.

Intact gastrolith sample for solid state NMR characterization. A piece was clipped off (100–200 mg) and packed into a 4- or 5-mm zirconia rotor after minimal grinding to enable stable spinning. Solid state NMR examination of intact gastroliths after extended periods of 6 mo and longer showed only ACC without any detectable crystalline phase. For fractured gastroliths, onset

of crystallization was detectable by the solid state NMR measurements after 1 mo.

Gastrolith decalcification. A fraction of a gastrolith was weighed (up to 200 mg) and immersed in a known volume of 0.5 M EGTA solution (approximately 20 mL/gr gastrolith) adjusting the pH to 7–8 with NaOH and HCl solutions throughout decalcification (7 d). The dissolved $CaCO_3$ and matter within it created a solution denoted soluble matrix. A fraction of this solution (600–700 μL) was subjected to solution NMR characterization (quantitative and semiquantitative measurements). This solution is denoted *gastrolith-EGTA*. The remaining solid, the chitin scaffold and nonsoluble matter, is denoted the insoluble matrix (Fig. 1*E*). This solid was collected by rinsing with water followed by overnight lyophilization or a week in desiccators, packed into a zirconia rotor and subjected to solid state NMR characterization. Additional decalcification procedure was employed by dissolving the gastrolith in an acidic solution of HCl (37% vol/vol). This acidic treatment, in addition to dissolving the $CaCO_3$, also hydrolyzes the chitin scaffold (49) and therefore may lead to dissolution of matter that otherwise was inaccessible to EGTA decalcification. This dissolution occurs within approximately 1 h for a 100-mg sample (final pH 2–3). The filtered solution was subjected to solution NMR measurements. The solutions from this procedure, denoted *gastrolith-HCl*, were used to confirm the identity of the molecular species probed in the soluble matrix (*gastrolith-EGTA*) in a simpler chemical environment avoiding the intense spectral background by EGTA.

Solid State and Solution NMR. Solid state 75-MHz ^{13}C and 121-MHz ^{31}P NMR measurements were carried out on two 300-MHz, triple-channel, solid state NMR spectrometers—*CMX-infinity* (Chemagnetics/Varian) and *AVANCE III* (Bruker), equipped with triple-resonance probes using 5- and 4-mm zirconia rotors, respectively. Samples were spun at 5,000 ± 2 Hz. CP MAS echo experiments were carried out with 5.0 and 10.0 μs $\pi/2$ and π pulse widths, an echo interval, τ (200 μs), identical to the rotor period T_R, a ^1H decoupling level of 100 kHz, Hartmann–Hahn rf levels were matched at 50 kHz, with contact times of 1–4 and 0.7–2 ms, and relaxation delays of 1.5–3 and 2–4 s for ^{13}C and ^{31}P, respectively. ^{13}C DE MAS echo experiments were carried out employing the same pulse parameters, however, with repetition delay of 2,400 s to ensure fully relaxed, quantitative spectra.

$^{13}C\{^{31}P\}$ REDOR experiments were conducted using a REDOR pulse sequence with refocusing π pulses after each rotor period (T_R) on the observed channel (^{13}C) and dephasing π pulses in the middle of each rotor period on the nonobserved nucleus (^{31}P), followed by an additional $2T_R$ period with a π-pulse in the middle to form simultaneously Hahn and rotational echoes. REDOR π-pulses employed xy-8 phase cycling for the refocusing and recoupling pulses (50, 51). Data acquisition employed an alternating block scheme, collecting a single S_0 transient with recoupling pulses turned off, followed by S_R transient collection with recoupling pulses turned on. Each part was processed (with 40-Hz line broadening) to yield the respective spectrum. REDOR difference spectra, ΔS, obtained via $S_0 - S_R$ subtraction exclusively exhibit peaks of dipolar-coupled chemical species. The REDOR data presented in the manuscript were collected using the CP excitation scheme.

A 2D-HETCOR $^{13}C\cdots^{31}P$ experiment was run employing $24 \times 24T_R$ TEDOR mixing (52). This experimental scheme (*SI Text*) starts with $^1H \rightarrow {}^{31}P$ CP (using the same parameters as for the ^{31}P CP MAS spectra above) followed by a t_1 evolution period in which the isotropic chemical shift of the ^{31}P is encoded; t_1 was incremented 36 times, with $\Delta t = 0.2$ ms $(=T_R)$. The subsequent TEDOR mixing is made up of $24T_R$ REDOR dipolar recoupling blocks in the preparation and buildup periods, i.e., before and after the (central) coherence transfer step via the two back-to-back $\pi/2$-pulses (on the ^{31}P and ^{13}C nuclei). In the $24T_R$ TEDOR preparation the refocusing π-pulses are on the ^{31}P channel (recoupling pulses in the middle of each rotor period on the ^{13}C channel), and in the $24T_R$ buildup period they are on the ^{13}C channel (recoupling pulses on the ^{31}P). Similar to the REDOR sequence above, an additional $2T_R$ period with a π-pulse in the middle is added to form simultaneously a Hahn and a rotational echo.

The chemical shifts of ^{13}C and ^{31}P are reported relative to tetramethylsilane, and 85% H_3PO_4, respectively, within ±0.1 ppm. REDOR simulations were performed using SIMPSON (53). Peak areas were calculated by deconvolution using DMFIT (54) and Topspin.

Solution NMR spectra were acquired on three different Bruker spectrometers at room temperature, all with two-channel, direct detection probes with automatic tuning and matching and equipped with z gradients: (*i*) *AV-III* 600 with resonance frequencies for ^1H, ^{31}P, and ^{13}C of 600.55, 243.11, and 151.03 MHz, respectively; (*ii*) *AV* 500 with resonance frequencies for ^1H and ^{13}C of 500.13 and 125.77 MHz, respectively; (*iii*) *AV-III* 400 with resonance frequencies for ^1H, ^{31}P, and ^{13}C of 400.40, 162.08, and 100.69 MHz, respectively. Bruker Topspin 2.1 was used on a personal computer (Windows-XP) for spectral acquisition and processing. The experimental details, spectra, and data analysis that served to identify and quantify the small MW content of the gastrolith are described in *SI Text*.

ACKNOWLEDGMENTS. We thank Prof. Aharon Loewenstein, Dr. Jayanthi Sundaresan, and Mr. Amichai Tal for stimulating discussions, Mr. William Tyler Winick (summer student, Scitech2010, Technion) for solution NMR measurements of EGTA. This study was supported in part by the Russell Berrie Nanotechnology Institute, Technion, by Israel Science Foundation Grants 1345/11 and 1080/05, and by German Israel Foundation Grant 950-9.5/2007.

1. Aizenberg J, et al. (2005) Skeleton of *Euplectella sp.*: Structural hierarchy from the nanoscale to the macroscale. *Science* 309:275–278.
2. Smith BL, et al. (1999) Molecular mechanistic origin of the toughness of natural adhesives, fibres and composites. *Nature* 399:761–763.
3. Mann S (2001) *Biomineralizatiom Principles and Concepts in Bioinorganic Materials Chemistry,* eds RG Compton, SG Davies, and J Evans (Oxford Univ Press, New York).
4. Gebauer D, Volkel A, Colfen H (2008) Stable prenucleation calcium carbonate clusters. *Science* 322:1819–1822.
5. Nagasawa H (2004) Macromolecules in biominerals of aquatic organisms. *Thalassas* 20:15–24.
6. Hattan SJ, Laue TM, Chasteen ND (2001) Purification and characterization of a novel calcium-binding protein from the extrapallial fluid of the mollusc, *Mytilus edulis. J Biol Chem* 276:4461–4468.
7. Marsh ME, Sass RL (1984) Phosphoprotein particles: Calcium and inorganic phosphate binding structures. *Biochemistry* 23:1448–1456.
8. Lowenstam HA, Weiner S (1989) *On Biomineralization*, eds HA Lowenstam and S Weiner (Oxford Univ Press, New York) p 324.
9. Addadi L, Raz S, Weiner S (2003) Taking advantage of disorder: Amorphous calcium carbonate and its roles in biomineralization. *Adv Mater* 15:959–970.
10. Weiss IM, Tuross N, Addadi L, Weiner S (2002) Mollusc larval shell formation: Aamorphous calcium carbonate is a precursor phase for aragonite. *J Exp Zool* 293:478–491.
11. Politi Y, et al. (2006) Structural characterization of the transient amorphous calcium carbonate precursor phase in sea urchin embryos. *Adv Funct Mater* 16:1289–1298.
12. Nicar MJ, Pak CY (1985) Calcium bioavailability from calcium carbonate and calcium citrate. *J Clin Endocrinol Metab* 61:391–393.
13. Meiron OE, et al. (2010) Solubility and bioavailability of stabilized amorphous calcium carbonate. *J Bone Miner Res* 26:364–372.
14. Politi Y, et al. (2010) Role of magnesium ion in the stabilization of biogenic amorphous calcium carbonate: A structure-function investigation. *Chem Mater* 22:161–166.
15. Li H, Xin HL, Muller DA, Estroff LA (2009) Visualizing the 3D internal structure of calcite single crystals grown in agarose hydrogels. *Science* 326:1244–1247.
16. Finnemore AS, et al. (2009) Nanostructured calcite single crystals with gyroid morphologies. *Adv Mater* 21:3928–3932.
17. Bentov S, Weil S, Glazer L, Sagi A, Berman A (2010) Stabilization of amorphous calcium carbonate by phosphate rich organic matrix proteins and by single phosphoamino acids. *J Struct Biol* 171:207–215.
18. Al-Sawalmih A, Li CH, Siegel S, Fratzl P, Paris O (2009) On the stability of amorphous minerals in lobster cuticle. *Adv Mater* 21:4011–4015.
19. Gertman R, Ben Shir I, Kababya S, Schmidt A (2008) In situ observation of the internal structure and composition of biomineralized Emiliania huxleyi calcite by solid-state NMR spectroscopy. *J Am Chem Soc* 130:13425–13432.
20. Taylor AR, Russell MA, Harper GM, Collins TFT, Brownlee C (2007) Dynamics of formation and secretion of heterococcoliths by Coccolithus *Pelagicus ssp braarudii. Eur J Phycol* 42:125–136.
21. Jahren AH, Skinner HCW (2007) Biogeochemistry. *Biomineralization*, ed WH Schlesinger (Elsevier Science, Oxford), Chap 4, Revised, 2nd Ed, Vol 8,, pp 1–69.
22. Luquet G, Marin F (2004) Biomineralisations in crustaceans: Storage strategies. *Comptes Rendus Palevol* 3:515–534.
23. Travis DF (1963) Structural features of mineralization from tissue to macromolecular levels of organization in decapod crustacea. *Ann N Y Acad Sci* 109:177.
24. Greenaway P (1985) Calcium balance and molting in the crustacea. *Biol Rev Camb Philos Soc* 60:425–454.
25. Shechter A, et al. (2008) Reciprocal changes in calcification of the gastrolith and cuticle during the molt cycle of the red claw crayfish Cherax quadricarinatus. *Biol Bull* 214:122–134.
26. Scott D, Duncan KW (1967) The function of freshwater crayfish gastroliths and their occurrence in perch, trout, and shag stomachs. *N Z J Mar Freshwat Res* 1:99–104.
27. Huxley TH (1880) *The Crayfish: An Introduction to the Study of Zoology,* International Scientific Series (D. Appleton and Company, New York), Vol XXVIII.
28. Shechter A, et al. (2008) A gastrolith protein serving a dual role in the formation of an amorphous mineral containing extracellular matrix. *Proc Natl Acad Sci USA* 105:7129–7134.
29. Takagi Y, Ishii K, Ozaki N, Nagasawa H (2000) Immunolocalization of gastrolith matrix protein (GAMP)in the gastroliths and exoskeleton of crayfish, *Procambarus clarkii. Zool Sci* 17:179–184.

30. Ishii K, Yanagisawa T, Nagasawa H (1996) Characterization of a matrix protein in the gastroliths of the crayfish *Procambarus clarkii. Biosci Biotechnol Biochem* 60:1479–1482.
31. Ishii K, Tsutsui N, Watanabe T, Yanagisawa T, Nagasawa H (1998) Solubilization and chemical characterization of an insoluble matrix protein in the gastroliths of a crayfish, *Procambarus clarkii. Biosci Biotechnol Biochem* 62:291–296.
32. Glazer L, et al. (2010) A protein involved in the assembly of an extracellular calcium storage matrix. *J Biol Chem* 285:12831–12839.
33. Sato A, et al. (2011) Glycolytic intermediates induce amorphous calcium carbonate formation in crustaceans. *Nat Chem Biol* 7:197–199.
34. Michel FM, et al. (2008) Structural characteristics of synthetic amorphous calcium carbonate. *Chem Mater* 20:4720–4728.
35. Gebauer D, et al. (2010) Proto-calcite and proto-vaterite in amorphous calcium carbonates. *Angew Chem Int Ed Engl* 49:8889–8891.
36. Jager C, Colfen H (2007) Fine structure of nacre revealed by solid state ^{13}C and ^{1}H NMR. *CrystEngComm* 9:1237–1244.
37. Nebel H, Neumann M, Mayer C, Epple M (2008) On the structure of amorphous calcium carbonate—A detailed study by solid-state NMR spectroscopy. *Inorg Chem* 47:7874–7879.
38. Lam RSK, Charnock JM, Lennie A, Meldrum FC (2007) Synthesis-dependant structural variations in amorphous calcium carbonate. *CrystEngComm* 9:1226–1236.
39. Hasse B, Ehrenberg H, Marxen JC, Becker W, Epple M (2000) Calcium carbonate modifications in the mineralized shell of the freshwater snail *Biomphalaria glabrata*. *Chemistry* 6:3679–3685.
40. Levi-Kalisman Y, Raz S, Weiner S, Addadi L, Sagi I (2002) Structural differences between biogenic amorphous calcium carbonate phases using X-ray absorption spectroscopy. *Adv Funct Mater* 12:43–48.
41. Jang MK, Kong BG, Jeong YI, Lee CH, Nah JW (2004) Physicochemical characterization of α-chitin, β-chitin, and γ-chitin separated from natural resources. *J Poly Sci A* 42:3423–3432.
42. Hu Y, Rawal A, Schmidt-Rohr K (2010) Strongly bound citrate stabilizes the apatite nanocrystals in bone. *Proc Natl Acad Sci USA* 107:22425–22429.
43. Fyfe CA, Mueller KT, Grondey H, Wongmoon KC (1992) Dipolar dephasing between quadrupolar and spin-1/2 nuclei. REDOR and TEDOR NMR experiments on VPI-5. *Chem Phys Lett* 199:198–204.
44. Jaroniec CP, Filip C, Griffin RG (2002) 3D TEDOR NMR experiments for the simultaneous measurement of multiple carbon-nitrogen distances in uniformly ^{13}C, ^{15}N-labeled solids. *J Am Chem Soc* 124:10728–10742.
45. Jehle S, et al. (2010) Intermolecular protein-RNA interactions revealed by 2D 31P-15N magic angle spinning solid-state NMR spectroscopy. *J Am Chem Soc* 132:3842–3846.
46. Toke O, Maloy WL, Kim SJ, Blazyk J, Schaefer J (2004) Secondary structure and lipid contact of a peptide antibiotic in phospholipid Bilayers by REDOR. *Biophys J* 87:662–674.
47. Raz S, Testeniere O, Hecker A, Weiner S, Luquet G (2002) Stable amorphous calcium carbonate is the main component of the calcium storage structures of the crustacean Orchestia cavimana. *Biol Bull* 203:269–274.
48. Shechter A, et al. (2007) Search for hepatopancreatic ecdysteroid-responsive genes during the crayfish molt cycle: From a single gene to multigenicity. *J Exp Biol* 210:3525–3537.
49. Einbu A, VÃ¥rum KM (2007) Depolymerization and de-N-acetylation of chitin oligomers in hydrochloric acid. *Biomacromolecules* 8:309–314.
50. Gullion T, Schaefer J (1989) Rotational-echo double-resonance NMR. *J Magn Reson* 81:196–200.
51. Gullion T, Schaefer J (1989) Detection of weak heteronuclear dipolar coupling by rotational echo double resonance nuclear magnetic resonance. *Adv Magn Reson* 13:57–83.
52. Hing AW, Vega S, Schaefer J (1992) Transferred-echo double-resonance NMR. *J Magn Reson* 96:205–209.
53. Bak M, Rasmussen JT, Nielsen NC (2000) SIMPSON: A general simulation program for solid-sate NMR spectroscopy. *J Magn Reson* 147:296–330.
54. Massiot D, et al. (2002) Modelling one- and two-dimensional solid-state NMR spectra. *Magn Reson Chem* 40:70–76.